Fatigue properties and cracking mechanisms of a 7075 aluminum alloy under axial and torsional loadings

Yizhuo Li, Delphine Retraint, H. Xue, T. Gao, Zhidan Sun

HAL Id: hal-02453428

https://utt.hal.science/hal-02453428

Submitted on 21 Jul 2022

Fatigue Design 2019

Fatigue properties and cracking mechanisms of a 7075 aluminum alloy under axial and torsional loadings

Y. Li[a], D. Retraint[a], H. Xue[b], T. Gao[b], Z. Sun[a,*]

[a]ICD, P2MN, LASMIS, Université de Technologie de Troyes (UTT), CNRS, Troyes, France
[b]Key Laboratory of Contemporary Design and Integrated Manufacturing Technology of Ministry of Education, Northwestern Polytechnical University, 127 West Youyi Road, Xi'an, China

Abstract

In this work, the fatigue properties of a 7075 aluminum alloy under axial and torsional loadings are investigated. For this purpose, fully reversed tension-compression as well as torsional fatigue tests were respectively conducted for polished dumbbell shaped specimens. The results of the tension-compression fatigue tests are first presented in the form of S-N plot, and the Basquin's equation is used to describe the fatigue data. Based on fatigue design, the fatigue data obtained under axial loading are transformed to estimate the life for torsional fatigue by determining equivalent shear stress using common failure criteria including Tresca, von Mises and maximum principal stress. The curves predicted using these criteria are compared to the experimental data obtained under torsional loading. Scanning Electron Microscopy (SEM) was used to observe the fracture surfaces in order to examine the crack initiation and propagation process. Fracture surfaces are presented at both macroscopic and microscopic scales and failure modes are discussed with regards to the failure criteria commonly used for fatigue life prediction.

*Keywords:*Aluminum alloy, Axial fatigue, Torsional fatigue, Fatigue life, Fracture surface

* Corresponding author. Tel.: +33-3-25-71-80-62
 E-mail address: zhidan.sun@utt.fr

1. Introduction

Aluminum alloys are widely used in the aircraft industry due to their high strength-to-density ratio. Extensive studies have been conducted to understand the fatigue behavior of aluminum alloys over the past decades. Most experimental studies on aluminum alloys were performed under uniaxial loading, and little torsional data can be found. However, the mechanical properties under cyclic torsional loading are important since many in service industrial components are subjected to torsional loading conditions.

In fatigue design process, shear fatigue properties of aluminum alloys are often estimated from axial data using failure criteria such as stress equivalent theories. Such criteria are often used because axial tests are much more accessible than torsional ones. However, before applying these criteria to predict fatigue life for mechanical parts under torsional loading, cracking process should be thoroughly studied for various materials due to the fact that the damage mechanisms might be different depending on the material. In the literature, some works have been performed to study fatigue behavior and damage mechanisms of different materials under both axial and torsional loadings. For example in the work of McClaflin and Fatemi (Mcclaflin, 2004), the authors investigated torsional deformation and fatigue behavior of a high strength spring steel. The stress-life (S-N) approach and strain-life curve based on commonly used failure criteria were evaluated by incorporating the examination of fracture mode. In some works about aluminum alloys, Marini & Ismail (Marini, 2011) conducted similar study on torsional fatigue behavior of a 6061 aluminum alloy. Some failure criteria were used based on S-N curve to evaluate their prediction capacity. Fractographic examination was performed to analyze the failure mechanisms for some typical fracture surfaces. In other works conducted by Zhang et al. (Zhang, 2011; Zhang, 2012), they investigated the fatigue behavior by emphasizing the analysis of fatigue failure under tension-torsion and non-proportional high cycle fatigue for a 2A12-T4 aluminum alloy. As for 7075 aluminum alloys, some studies have been conducted for torsional fretting fatigue, for example by focusing on damage evolution (Peng, 2018). Even some studies have been performed, as mentioned above, torsional fatigue of aluminum alloys is always an interesting topic. The fatigue properties should be thoroughly studied by associating the investigation of damage mechanisms. Based on these information, a powerful prediction tools could be finally built, which will make engineering work more efficient while designing mechanical parts under fatigue loading.

In this paper, the fatigue properties of a 7075 aluminum alloy are investigated through experiments under tension-compression and torsional loadings. First, the material characteristics and the experimental procedure are briefly presented in Section 2. Then, in Section 3 concerning the description of the results, the obtained fatigue data are presented in form of S-N plot. Fatigue life prediction for torsion condition is also given based on the results obtained with axial tension-compression loading. The predicted S-N curves are compared to experimental data of torsional fatigue tests. Furthermore, fatigue cracking mechanisms are analyzed by observing the fracture surfaces in both macroscopic and microscopic scales. These fracture surface observations allow to understand the damaging process of the material under both tension-compression and torsional loadings. Finally based on these analyses, some concluding remarks are given in Section 4.

2. Material and experimental procedure

2.1. Material

A commercial 7075 aluminum alloy was investigated in this work. It is a high-strength heat-treated aluminum alloy whose typical application is in aircraft structures or light-weight structures. This alloy has a good combination of mechanical resistance and low environmental impact for transport applications. The material was received in form of extruded bars with a diameter of 15 mm. Its nominal chemical composition (in wt%) is given as follows: 5.1-6.1Zn, 2.1-2.9Mg, 1.2-2Cu, 0.18-0.28-Cr, max 0.5Fe, max 0.4Si, max 0.2Ti, max 0.3 Mn, and balance Al. The microstructure observed using Optical Microscopy (OM) shows the presence of dendritic arms in the transverse section (Fig. 1a). In the longitudinal section, however, stripe-kind features can be observed, which indicates that the material was strongly extruded during its elaboration process. Very similar microstructure was reported by Trsko et al. (Trsko, 2014) for an AW 7075 alloy. In addition, microstructure observation coupled with Energy Dispersive X-Ray Spectroscopy (EDS)

analysis shows that a great number of inclusions are also present and they are especially visible in the longitudinal section (Fig. 1b). In their study for a 7075 aluminum alloy, Singh et al. (Singh, 2015) revealed that the inclusions correspond to Al_7Cu_2Fe and Mg_2Si intermetallics. These intermetallic particles could have harmful effect on fatigue life of 7075 alloys, since these alloys are particularly sensitive to microstructural inclusions that can cause local stress concentration.
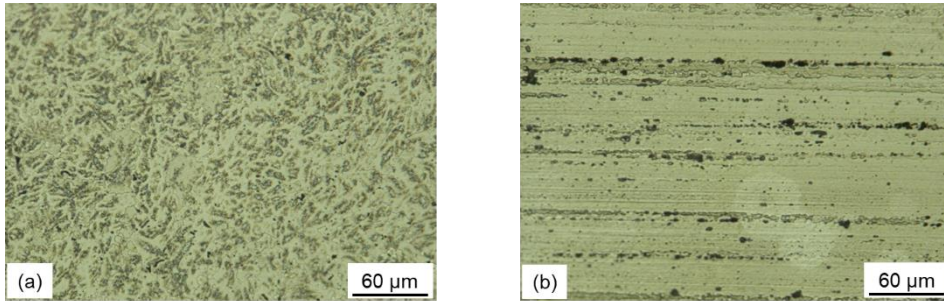

Fig. 1. Metallographic observation of the studied 7075 aluminum alloy on (a) transverse section, and (b) longitudinal section. Note that there is the presence of a great number of intermetallic inclusions especially visible on the longitudinal section.

2.2. Experimental procedure

For both tension-compression and torsional fatigue tests, the specimens with the same geometry and dimensions are used, as shown in Fig. 2. For the torsional fatigue tests, there has often been a discussion as to whether there is a difference in the fatigue behavior between cylindrical solid specimens and thin-walled tube ones (McClaflin, 2004). Thin-walled tubes are more expensive and difficult to manufacture accurately. Stress calculations for such specimens are, however, straightforward due to nearly uniform stresses over the wall thickness. While solid specimens are easier to manufacture, and it is more difficult to perform stress calculations because of the presence of the stress gradient from the center to the surface of specimen. In the literature, solid specimens have been also largely used (Jiang, 2018; Zhang, 2012), and the calculation of shear stress (when the specimens are only elastically deformed) is based on this relation $\tau = 16T/\pi d^3$. In this equation, T is the applied torque amplitude and d is the central diameter of the specimen.

As for the conditions of the fatigue tests, the specimens were tested under fully reversed loading (load ratio R =-1) for both tension-compression and torsional fatigue. The experiments were conducted by using a sinusoidal waveform under constant amplitude loading at room temperature. The load amplitudes were chosen so that the fatigue lives are in the range of high cycle fatigue (between 3×10^4 and 2×10^6 cycles in this work). For all the fatigue tests, fatigue failure is defined as the complete rupture of the specimen. An ElectroPuls tension-torsion fatigue machine was used to perform these tests. The fatigue machine has a capacity of 100 Nm in torque and 10 kN in axial load. Fatigue tests were carried out under tension-compression stress control with a frequency of 20 Hz, and under shear stress control with a frequency of $f = 4$ Hz. In the case of torsional tests, to ensure an accurate alignment of the specimen with the machine, a specially designed grip alignment system was used while mounting the specimen. It is worth mentioning that for the torsional fatigue tests, the axial channel of the machine was in load control, which allowed the specimens to change in length and avoid any axial stress due to specimen dilatation.
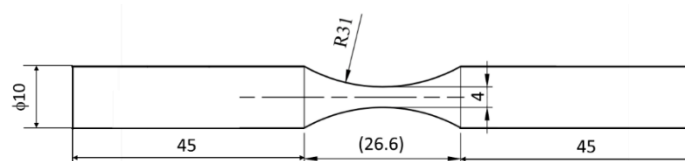

Fig. 2. Geometry and dimensions of the fatigue specimen used in this work for both tension-compression and torsion loadings.

3. Results and discussion

3.1. Fatigue life analysis

The obtained fatigue test data are first presented in the form of S-N plot, as shown in Fig. 3. The S-N (stress-life) approach is often used for fatigue design of structural materials subjected to high cycle fatigue, where small or no plastic deformation exists. Note that to directly apply Basquin'equation, the horizontal axis is expressed as the number of reversals to failure, i.e. twice number of cycles to failure N_f. From Fig. 3, it can be seen that there is a clear trend for the data points distribution. To model this trend and predict the fatigue life, the Basquin's equation with the form $\sigma_{N_f} = \sigma_f'\left(2N_f\right)^b$ is used. In this equation, σ_f' is the fatigue strength coefficient and b is the fatigue strength exponent. It should be noted that for this small number of the obtained data points, there is already a high dispersion, especially in the range of low stress amplitudes. However, in the range of high stress amplitude (between 315 and 330 MPa), it seems that the several data points give a clear tendency without great scatter. This observation about the scatter of fatigue lives is consistent with the opinion generally accepted in the literature, i.e. the scatter tends to be high when the stress amplitude is decreased. For the material studied in this work, the large scatter of the fatigue lives might be mainly due to the heterogeneous distribution of microstructural defects such as intermetallic inclusions, as highlighted in Section 2.1. This significant scatter means that the prediction using the Basquin's equation based on these data points could not be highly reliable. A more reasonable way to improve the prediction accuracy is to multiply the number of fatigue tests and then use a statistical method to give a more comprehensive analysis. However, the main goal of this paper is to present the preliminary investigation about the fatigue properties of 7075 aluminum alloy under both tension-compression and torsional loadings. In addition, a particular attention will be given to the link between tension-compression fatigue and torsional fatigue for this alloy.
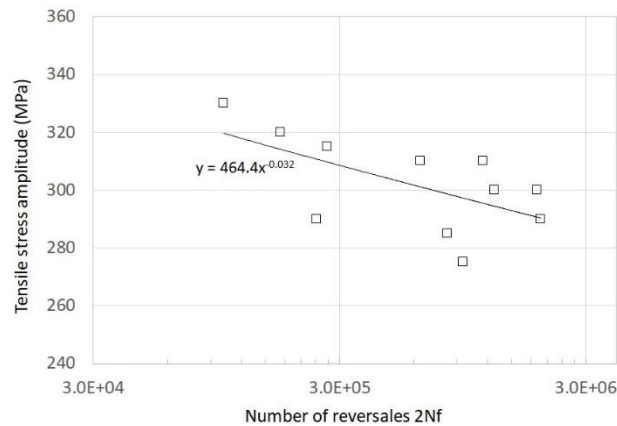

Fig. 3. S-N plot of for the tension-compression fatigue tests. The experimentally obtained data points are described by a Baquin's equation.

For this purpose, the results obtained under tension-compression loading were used to estimate the fatigue life for torsional fatigue by determining the equivalent shear stress using one of the common failure criteria such as Tresca ($\tau_{N_f} = \sigma_{N_f}/2$), Mises ($\tau_{N_f} = \sigma_{N_f}/\sqrt{3}$), and maximum principal stress ($\tau_{N_f} = \sigma_{N_f}/(1 + \nu)$, with ν being Poisson's ratio). Each of the three criteria was used to build an S-N curve, and the curve was compared to the experimental data, as shown in Fig. 4. It can be seen that while none of these criteria result in very satisfactory predictions, the Mises criterion is closer to the experimental curve. The torsional fatigue strength at around 10^6 cycles predicted by using the Mises criterion is very close to the value obtained by the experimental curve obtained by torsional fatigue tests. This means that the fatigue life predicted using Mises criterion could be reliable in this range of number of cycles to failure. However, for the range less than 8×10^5 cycles, the fatigue life is under-predicted, and this under-prediction is increased with the increase of stress level. As for the other two criteria, choosing them would result in very poor predictions. Using maximum principal stress would have a highly over-estimated fatigue life, while applying Tresca criterion would give a strongly under-estimated prediction. It should be noted that in the absence of experimental torsional fatigue data, one would choose the Mises criterion for this alloy, according to the results presented above.

The fact that one criterion is more suitable than others is rather determined by the damage mechanisms of the material under both tension-compression and torsional loadings. Thus in the following sections, some representative fracture surfaces will be presented in order to clarify this point.
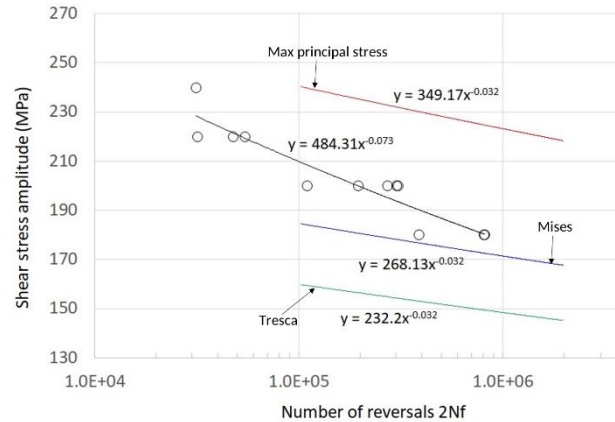

Fig. 4. Fatigue life predictions using three different criteria respectively shown by the red, blue and green curves based on tension-compression fatigue test data. Experimental torsional fatigue data (black circles) and its curve fitted using Basquin's equation (black curve) are also given.

3.2. Fracture profiles of specimens

From the experimental viewpoint, it is generally accepted that the cracking begins at a hot spot, continues with a crack initiation phase (Stage I) near the maximum shear stress direction, and subsequently proceeds to a propagation phase near the maximum principal stress direction (Stage II). In the case of high cycle fatigue, the fatigue life proportion represented by the crack initiation phase is dominant (more than 90% of the total fatigue life). To reveal the cracking process, the lateral fracture profiles were observed using a numerical microscope and the fracture surfaces were observed using a Scanning Electron Microscope (SEM). A series of micrographs was taken in order to study the cracking mechanisms. Special attention was paid to where the fatigue crack initiated and what is the difference between the cracking processes under tension-compression and torsional loadings with different stress levels.

Some typical fracture profiles of broken specimens obtained under tension-compression and torsion loadings are shown in Fig. 5. It can be seen that the appearance of the facture profiles for these two fatigue loadings is fundamentally different. As a matter of fact, the fracture profiles obtained under tension-compression is very "rugged" (Figs. 5a and 5b), whereas the ones obtained under torsional loading is quite "flat" and they are almost perpendicular to the specimen axis for all the cases studied in this work (Figs. 5c and 5d). This significant difference in fracture appearance means that the cracking mode is strongly different under the two different loading modes. Note that under torsional loading, the direction of shear stress is within a horizontal plane, i.e. perpendicular to the axis of the specimen. Therefore, the crack orientations are consistent with the direction of shear stress. This seems to indicate that macroscopically shear stress dominates the torsional fatigue failure for this alloy. Very similar facture surfaces were obtained for others aluminum alloys such as 2A12-T4 tested by Zhang et al. (Zhang, 2011).
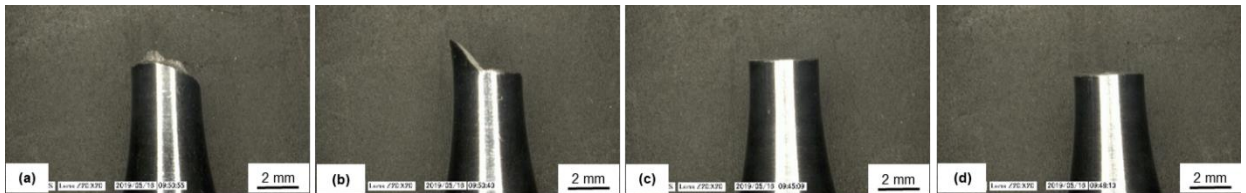

Fig. 5. Typical cracking profiles obtained under: (a) tension-compression with low stress amplitude ($\sigma_a = 290$ MPa), (b) tension-compression with high stress amplitude ($\sigma_a = 330$ MPa), (c) torsion with low shear stress amplitude ($\tau_a = 180$ MPa) and (d) torsion with high stress amplitude ($\tau_a = 220$ MPa).

3.3. Fracture surface analysis

The global view of a typical fracture surface obtained under tension-compression is illustrated in Fig. 6a. It can be seen that three cracking regions can be easily distinguished. They correspond respectively to crack initiation region, crack propagation region and final rupture region. Furthermore, under tension-compression fatigue, most cracks initiated at or near the surfaces of the specimens. Under tension-compression loading, when the stress amplitude is high (σ_a = 330 MPa), there are two crack initiation sites, as indicated by arrows in Fig. 6a. A main crack was first initiated at the specimen surface. Then there was a propagation stage of short crack during which the crack growth speed is slow. The fracture surface appearance of this near crack initiation region is rather flat, as can be seen in Fig. 6b. This means that the crack propagated following small zig-zag path of low amplitude, and the global appearance of the obtained fracture surface is thus less rugged. For the propagation region of the main crack, there are several large visible river-like bands which divergently spread towards the interior of the specimen from the crack initiation region (Fig. 6a). At the large river-like bands (blue mark in Fig. 6a), the fracture is ductile since there are many dimples formed due to tensile and shear tearing (Fig. 6c). Between these large river-like bands (black mark in Fig. 6a), there are the presence of larger dark bands with many transgranular facets more or less crystallographic (Fig. 6d). As a matter of fact, these features of river-like bands and dark bands between them signify that there were multi crack fronts and the river-like bands were formed due to the junction of multi crack fronts during the main crack growth. Apart from the main crack, another crack also initiated from the specimen surface (Fig. 6a). It is believed that during the propagation of these two cracks, they joined each other, which lead to the final brutal fracture of the specimen.
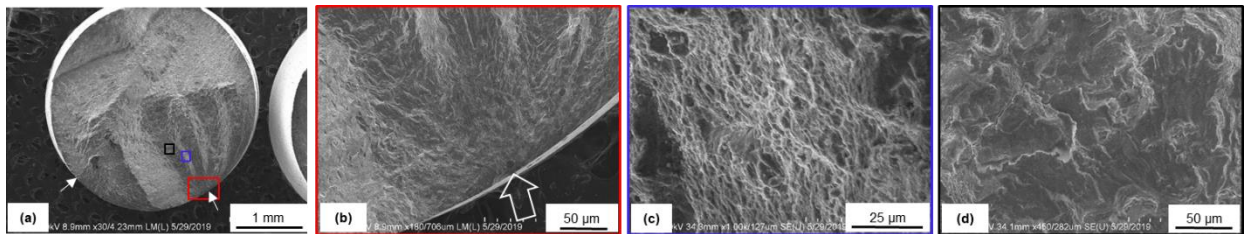

Fig. 6. Fracture surfaces obtained under tension-compression loading with high stress amplitude (σ_a= 330 MPa): (a) global view of fracture surface, (b) crack initiation region, (c) detailed observation of river-like bands, and (d) detailed observation of larger dark bands.

Under tension-compression loading with low stress amplitude, the fracture surface shown in Fig. 7 is basically similar to that obtained under high stress amplitude, i.e. the crack initiated at the specimen surface and propagated towards the interior with the companying of river-like bands (Fig. 7a). However, when the stress amplitude is even lower, the crack initiation site tends to shift to the near surface region and tends to have a single crack initiation site (Figs. 7c and 7e).
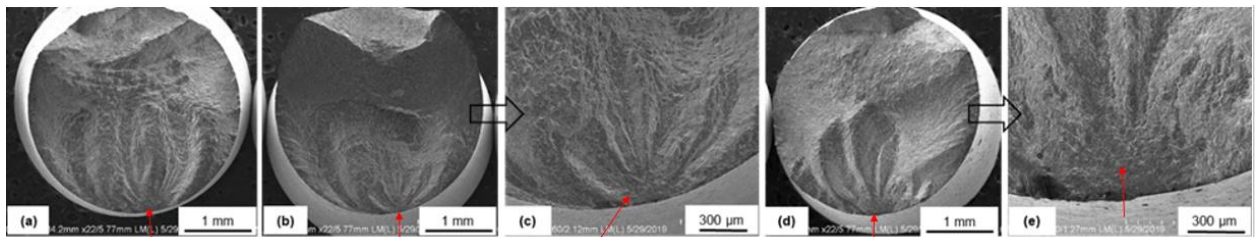

Fig. 7. Fracture surfaces obtained under tension-compression loading with lower stress amplitudes (red arrows approximately indicate crack initiation sites): (a) global view obtained under (σ_a =300 MPa), (b) global view obtained under (σ_a =290 MPa), (c) zoomed view of (b), (d) global view obtained under (σ_a =275 MPa), and (e) zoomed view of (d).

For the case of torsional fatigue, typical global fracture surface shows the presence of concentric ring-like features, as can be seen in Fig. 8a. Following the ring-like features, it is easy to identify their centre as the final rupture region. It can be seen that the final rupture region is quite small with respect to the entire fracture surface. Considering the nature of torsional loading, these ring-like features might be generated mainly due to shear stress loading. For some regions, there are traces caused by the friction between the surfaces of the two parts once they were separated by cracking. Through Fig. 8a, it is easy to discern that the fatigue crack initiated around the surface, as indicated by the arrow shown in the zoomed view (Fig. 8b). This observation is consistent with the fact that the maximum shear stress is located at the surface most far from the final rupture region. Note that the final rupture region served as the rotation centre, and it is not located at the geometrical centre of the specimen, according to the fracture surface. Similar observation about the location of the final rupture region was reported in the literature (Zhang, 2011). This shift of rotation centre from the geometrical centre of the specimen might be due to the misalignment of the specimen and/or the heterogeneous features of the material through the traverse section. However, further systematic study is needed to clarify this point.

Detailed microscopic observations were also performed in order to have deeper understanding of damage mechanisms. Fig. 8b shows that the fracture surface is quite flat and there is no much relief, which means that the fracture is rather transgranular and of brittle nature. This feature is more or less similar to the case of tension-compression loading. With the propagation of the crack, there was the occurrence of rugged surface features due to more ductile fracture. This is due to the fact that the crack propagation speed became more pronounced and the cracking process was accompanied by micro-tearing of material. In the region shown by Fig. 8b, several traces of abrasion are present, as indicated by blue arrows. These abrasion-induced traces were created due to reversed torsional loading during which the contact somewhere between the two separated surfaces was inevitable. Fig. 8c shows a micrograph of the crack propagation region where clear shear bands are present. They are formed due to the ductile rupture of the material under the effect of torsional shear stress. In addition, there is also the presence of vague fatigue striation in this region (see Fig. 8c), which witnesses the rapid step by step crack growth during steady fatigue crack propagation stage. As for the final rupture region, a typical micrograph is shown in Fig. 8d. Equiaxed small and large dimples are the main feature of this region, and the surface is rather rugged due to the strong ductile tearing that occurred during the final fracture process.
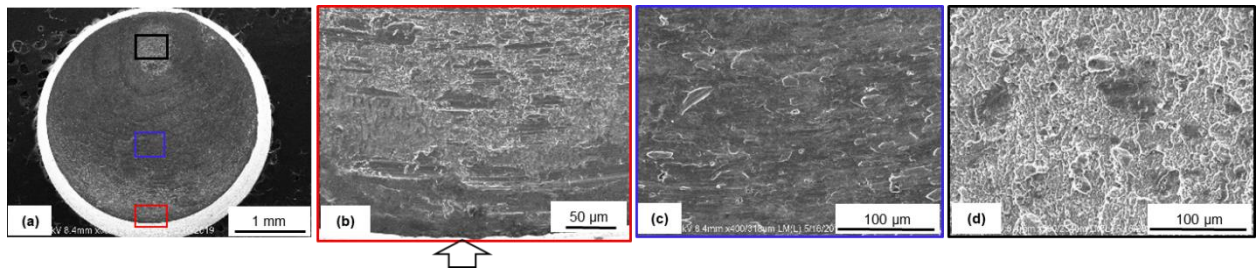

Fig. 8. Typical fracture surfaces obtained under torsional loading ($\tau_a = 220$ MPa): (a) global view of fracture surface, (b) crack initiation region (the arrow indicates the crack initiation site at the surface), (c) crack propagation region and (d) final rupture region.

4. Concluding remarks

In this work, the fatigue properties of a 7075 aluminium alloy under axial and torsional high cycle fatigue were investigated, and the fracture surfaces were observed to study the damage mechanisms, especially the cracking process of this aluminium alloy under tension-compression and torsional loadings. Based on the analysis of the results presented in this paper, the following including remarks could be retrained:

- A link between tension-compression fatigue and torsional fatigue was established by applying three failure criteria. Among these three criteria, the prediction using Mises corresponds more or less better to the experimental S-N data, while the other two criteria will over-estimate or under-estimate the fatigue limit if they are used in fatigue design.

- Under tension-compression fatigue, the crack initiated at the specimen surface and the obtained fracture profiles are very rugged. Under high stress amplitudes, multiple crack initiation sites tends to occur, whereas under low stress amplitudes, only single crack initiation site is present.
- Under torsional fatigue, the crack initiation occurred at the surface farthest from the rotation centre. Ring-like features are present, which are formed due to the effects of the shear stress and the abrasion between the two separated surfaces. These ring-like features converge towards the rotation centre region where the final rupture occurred. In this final rupture region, equiaxed dimples are present and they are formed due to local ductile rupture of the material.

Acknowledgements

References

Marini, M., & Ismail, A. (2011). Torsional deformation and fatigue behaviour of 6061 aluminium alloy. IIUM Engineering Journal, 12(6), 21–32.

Mcclaflin, D., & Fatemi, A. (2004). Torsional deformation and fatigue of hardened steel including mean stress and stress gradient effects. International Journal of Fatigue, 26, 773–784. https://doi.org/10.1016/j.ijfatigue.2003.10.019

Peng, J., Jin, X., Xu, Z., Zhang, J., Cai, Z., Luo, Z., & Zhu, M. (2018). Study on the damage evolution of torsional fretting fatigue in a 7075 aluminum alloy. Wear, 402–403, 160–168. https://doi.org/10.1016/j.wear.2018.02.008

Singh, S. S., Guo, E., Xie, H., & Chawla, N. (2015). Intermetallics Mechanical properties of intermetallic inclusions in Al 7075 alloys by micropillar compression. Intermetallics, 62, 69–75. https://doi.org/10.1016/j.intermet.2015.03.008

Trsko, L., Guagliano, M., Bokuvka, O. & Novy, F. (2014). Fatigue life of AW 7075 aluminium alloy after severe shot peening treatment with different intensities. Procedia Engineering, 74, 246–252. https://doi.org/10.1016/j.proeng.2014.06.257

Zhang, J., Shi, X., Bao, R., & Fei, B. (2011). Tension – torsion high-cycle fatigue failure analysis of 2A12-T4 aluminum alloy with different stress ratios. International Journal of Fatigue, 33(8), 1066–1074. https://doi.org/10.1016/j.ijfatigue.2010.12.007

Zhang, J., Shi, X., & Fei, B. (2012). High cycle fatigue and fracture mode analysis of 2A12 – T4 aluminum alloy under out-of-phase axial – torsion constant amplitude loading. International Journal of Fatigue, 38, 144–154. https://doi.org/10.1016/j.ijfatigue.2011.12.017

Zhao, T. & Jiang, Y. (2018). Fatigue of 7075-T651 aluminum alloy. International Journal of Fatigue, 30, 834-849. https://doi.org/10.1016/j.ijfatigue.2007.07.005